Ab Initio Modeling of Donor−Acceptor Interactions and Charge-Transfer Excitations in Molecular Complexes: The Case of Terthiophene−Tetracyanoquinodimethane

Juan Aragó,[†,‡] Juan C. Sancho-García,[§] Enrique Ortí,[*,†] and David Beljonne[‡]

[†]Instituto de Ciencia Molecular, Universidad de Valencia, E-46980 Valencia, Spain
[‡]Laboratory for Chemistry of Novel Materials, Université de Mons, Place du Parc 20, B-7000 Mons, Belgium
[§]Departamento de Química Física, Universidad de Alicante, E-03080 Alicante, Spain

Ⓢ Supporting Information

ABSTRACT: This work presents a thorough quantum chemical study of the terthiophene−tetracyanoquinodimethane complex as a model for π−π donor−acceptor systems. Dispersion-corrected hybrid (B3LYP-D) and double hybrid (B2PLYP-D), hybrid meta (M06-2X and M06-HF), and recently proposed long-range corrected (LC-wPBE, CAM-B3LYP, and wB97X-D) functionals have been chosen to deal with π−π intermolecular interactions and charge-transfer excitations in a balanced way. These properties are exhaustively compared to those computed with high-level ab initio SCS-MP2 and CASPT2 methods. The wB97X-D functional exhibits the best performance. It provides reliable intermolecular distances and interaction energies and predicts a small charge transfer from the donor to the acceptor in the ground state. In addition, wB97X-D is also able to yield an accurate description of the charge-transfer excitations in comparison to benchmark CASPT2 calculations.

■ INTRODUCTION

Donor−acceptor (D−A) molecular complexes, formed by π-conjugated materials, have recently attracted a large interest in the field of organic solar cells since these complexes can undergo very efficient photoinduced charge transfer (CT).[1,2] In addition to the charge generation process, optimum charge transport through donor and acceptor layers is essential to achieve high performances in solar energy conversion.[3] In this respect, donor and acceptor materials with fine-tuned semiconducting properties are also needed. Oligothiophenes (nTs) constitute one of the most widely studied classes of semiconducting materials acting as electron-donor compounds. They show suitable electronic and solid-state properties that result into high charge carriers mobilities.[4−7] On the other hand, 7,7,8,8-tetracyano-p-quinodimethane (TCNQ), acting as a strong electron-acceptor, has attracted special attention in the field of molecular materials since the discovery of the first true organic metal, namely, the CT complex formed by this molecule and tetrathiafulvalene.[8,9] Although both nTs and TCNQ derivatives have been well studied individually, D−A complexes formed by these systems have received much less attention.[10,11]

Recently, Panda et al. investigated a series of donor π-conjugated oligomers mixed with electron acceptors in chloroform by means of UV−vis absorption spectroscopy and cyclic voltammetry.[12] Compelling spectroscopic evidence for the formation of nTs−TCNQ D−A complexes in solution was provided. More specifically, new absorption bands were identified for mixtures of nTs and TCNQ in chloroform whose intensities showed a marked dependence on the concentration of the donor and the acceptor and did not match those reported for $[n$Ts$]^+$ and $[$TCNQ$]^-$. These new bands were described as electronic transitions from the ground state (no charge separation) to the charge-separated excited state of the nTs−TCNQ complexes. Although the complexes were experimentally detected, fundamental information about the geometry of the supramolecular dimer, the charge distribution in the electronic ground state, and the nature of the CT excitations is scarce. This information can be conveniently assessed from state-of-the-art quantum chemical calculations that are able to simultaneously describe van der Waals (dispersion) interactions and CT excitations in a balanced way.

Theoretically, the accurate treatment of both van der Waals interactions and CT excitations is a difficult and challenging task for most quantum chemical methods and is thus the subject of intense ongoing research. Dispersion interactions purely arise from electron correlation effects[13] and thus need highly correlated wave function methods to treat them adequately. Coupled-cluster theory with singles, doubles, and perturbatively connected triple excitations [CCSD(T)], in conjunction with large basis sets, can accurately describe these effects.[14,15] Unfortunately, CCSD(T) calculations are computationally very demanding and therefore unfeasible for systems such as D−A complexes of medium-size. On the other hand, second-order Møller−Plesset perturbation theory (MP2)[16] has a lower computational cost (N^5 vs N^7, where N is related to the size of the system) and can be accordingly seen as a suitable method to partly account for dispersive interactions in large systems. However, the MP2 method tends to generally overestimate binding energies for π-stacked systems.[17−19] Hence, an alternative to MP2 recently appeared, denoted as spin-component scaled MP2 (SCS-MP2), which significantly improves the MP2 results, namely, the

overestimation of the binding energies in π-stacks.[20,21] Therefore, the SCS-MP2 method can be considered as a reliable quantum chemical wave function method to treat noncovalent interactions in large π-systems where the cost of CCSD(T) is prohibitive.

We now turn our attention to Kohn–Sham (KS) density functional theory (DFT), which is by far the most widely used method for electronic structure calculations in condensed matter physics and quantum chemistry. It seems that a general drawback of all the common functionals is their inability to describe long-range electron correlations responsible for noncovalent interactions.[22−24] The long-range correlation effects can be captured by nonempirical approaches specially devised to account for dispersion interactions explicitly.[25−31] Another approach is to combine symmetry-adapted intermolecular perturbation theory (SAPT) with a DFT representation of the monomers.[32] Since this representation of dispersion interactions is nonempirical in nature, the computational cost still represents a serious bottleneck. In recent years, there has been considerable interest in a less costly yet qualitatively correct DFT-based description of noncovalent interactions, leading to several dispersion-corrected methods.[32−41] Among them, the new series of M06-class functionals developed by Truhlar and co-workers[33,34] has extensively been parametrized to take dispersive effects into account. The simplest approach, normally designated as DFT-D, introduces dispersion interactions using an empirical potential of the form $C_6R^{−6}$.[35−41] The dispersion energy is calculated separately from DFT calculations and simply added to the converged DFT energy. DFT-D has been applied to calculate the intermolecular interactions energies for large benchmark sets of noncovalent molecules with very satisfactory results.[42−44] Therefore, this approach can be an excellent alternative to deal with large systems such as those tackled here.

Another well-known shortcoming of DFT methodologies is the poor description of CT excitations for local and hybrid functionals traditionally used within the time-dependent DFT (TD-DFT) approach.[45] This shortcoming can be overcome using multiconfigurational ab initio methodologies, such as the complete active space method combined with a second-order perturbation approach (CASSCF/CASPT2). The CASSCF/CASPT2 method is the most appropriate for the study of CT excitations where TD-DFT fails totally.[46] However, the application of the CASSCF/CASPT2 protocol to large systems requires enormous computational resources. A recent promising alternative within the TD-DFT framework, which improves the accuracy of both Rydberg and CT excitations while maintaining good quality local excitations, is the long-range corrected approach (LC).[47] This approach consists in the splitting of the $1/r_{12}$ two-particle operator into short- and long-range exchange components, with the help of the standard error function (erf):

$$\frac{1}{r_{12}} = \frac{1 - \mathrm{erf}(\omega r_{12})}{r_{12}} + \frac{\mathrm{erf}(\omega r_{12})}{r_{12}} \qquad (1)$$

where r_{12} is the interelectronic distance and ω is a parameter defining the range separation. Short-range exchange is treated mainly using a local or hybrid functional, whereas long-range exchange is usually treated using exact orbital exchange. Within this LC scheme, several functionals, such as LC-wPBE,[48] Coulomb-attenuated CAM-B3LYP,[49,50] and the wB97[51−53] family have been recently proposed to improve CT excitation predictions. Double hybrid functionals, like B2PLYP, have also
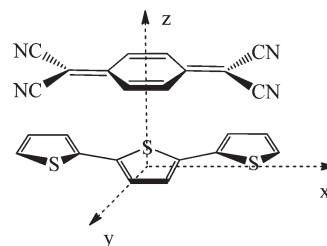

Figure 1. Terthiophene−tetracyanoquinodimethane complex in the cofacial geometry. The two molecular planes are parallel to one another.

shown very good performance in benchmark calculations for vertical excitation energies of a wide variety of organic molecules.[54,55] Furthermore, the combination of B2PLYP with the dispersion approach (B2PLYP-D) has been repeatedly tested to yield accurate noncovalent interactions.[43,44,56] Hence, this functional can also be seen as a robust and reliable alternative method.

Here we perform a thorough quantum chemical study of the terthiophene−tetracyanoquinodimethane (3T−TCNQ) complex (Figure 1) focusing mainly on: (i) the performance of several density functionals to account for the energetics of $\pi−\pi$ interactions between 3T and TCNQ, (ii) the charge distribution provided by the different functionals for the 3T−TCNQ ground-state, (iii) the identification and the characterization of the most stable structures, and (iv) the description of the nature and the energy of the CT excitations. In a broader perspective, our aim is thus to identify a suitable methodology that can both properly account for $\pi−\pi$ interactions and predict reliable CT excitation energies, which can be mostly useful to investigate larger $\pi−\pi$ D−A complexes.

■ THEORETICAL AND COMPUTATIONAL DETAILS

Calculations were performed with the Gaussian 09[57] and ORCA[58] program packages. Calculations make use of the cc-pVDZ and cc-pVTZ basis sets.[59] The former was chosen as a compromise between accuracy and applicability to large molecules. The isolated molecules, 3T and TCNQ, were first optimized using the Becke's three-parameter B3LYP exchange functional[60,61] and the cc-pVDZ basis set. Potential energy curves were constructed by plotting the intermolecular interaction energy between 3T and TCNQ monomers, in a purely cofacial geometry, and by varying the intermolecular distance between the molecular centers along the z axis (see Figure 1). The intermolecular interaction energy (ΔE) calculated by the different methods was computed as follows:

$$\Delta E = E_{3T−TCNQ} − E_{3T} − E_{TCNQ} \qquad (2)$$

where $E_{3T−TCNQ}$ denotes the energy of the complex and E_{3T} and E_{TCNQ} correspond to the energy of the monomers. The SCS-MP2 method in conjunction with the cc-pVTZ basis set will be used as reference for this part of the study due to its close agreement with CCSD(T) results.[21] Note that the correlation energy at second order is scaled according to the following equation:

$$E^{corr}(SCS − MP2) = p_S E_{\uparrow\downarrow} + p_T E_{(\uparrow\uparrow + \downarrow\downarrow)} \qquad (2)$$

where $E_{(\uparrow\uparrow+\downarrow\downarrow)}$ and $E_{\uparrow\downarrow}$ are the second-order contributions from double excitations of electron pairs with parallel- and antiparallel-spin, respectively, with $p_S = 6/5$ and $p_T = 1/3$ being the default scaling parameters.[20]
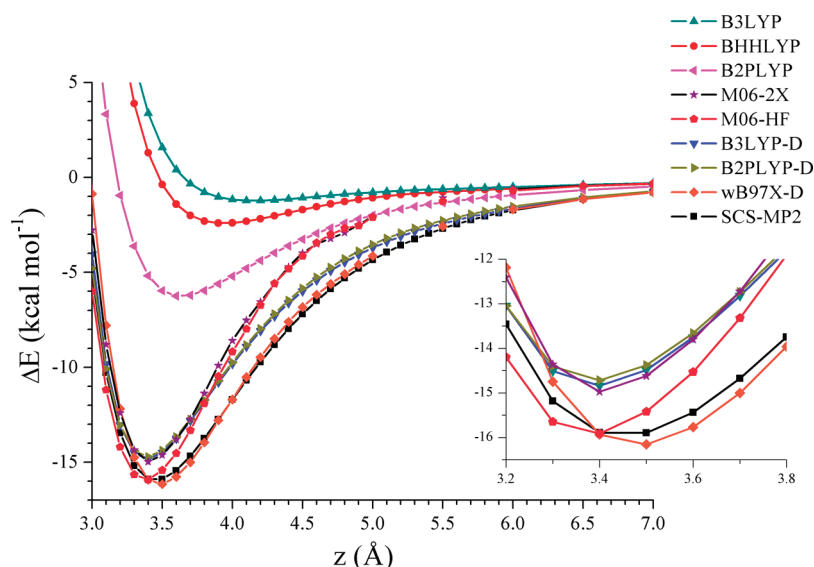
Figure 2. Potential energy curves for the cofacial 3T−TCNQ complex computed at various DFT/cc-pVDZ levels. The SCS-MP2/cc-pVTZ curve is shown as a reference. Intermolecular interaction energies (ΔE) are counterpoise uncorrected.

The interaction energy was then calculated at the B3LYP-(-D),[60,61] BHHLYP,[60,61] B2PLYP(-D),[62] M06-2X,[34] M06-HF,[63] and wB97X-D[52] levels in combination with the cc-pVDZ and cc-pVTZ basis sets. The -D term denotes the approach originally developed by Grimme to calculate the dispersion energy (E_D) between two weakly overlapping systems, which is calculated separately (in a post-self consistent field fashion) by resorting to a van der Waals-type function explicitly depending on the well-known R_{AB}^{-6} decay of such interactions:[38]

$$E_D = -s_6 \sum_{AB} f_d(R_{AB}) \frac{C_6^{AB}}{R_{AB}^6} \qquad (3)$$

where $f_d(R_{AB})$ is a damping function of the interatomic distance (R), C_6^{AB} is the dispersion coefficient for the atomic pair AB, and s_6 is a scaling factor that only depends on the functional used. The parameters implemented for B3LYP-D and B2PLYP-D in ORCA and for wB97X-D in Gaussian 09 were used as defaults.

Basis set superposition errors (BSSEs) for the interaction energies in the 3T−TCNQ complex were computed by applying the counterpoise (CP) method.[64]

The resolution of the identity (RI) technique[65,66] was employed for SCS-MP2 and B2PLYP calculations. The error introduced by the RI treatment is completely negligible compared to other effects. The terms SCS-MP2 and B2PLYP will be used instead of RI-SCS-MP2 and RI-B2PLYP, respectively.

The vertical CT excitation energies were first computed by means of the CASPT2 approach.[67−69] In this method, the first-order wave function and the second-order energy are calculated using the CASSCF wave function as reference. The CASSCF/CASPT2 protocol has been shown to be remarkably accurate for CT excitation energies of organic molecules which are not well described by TD-DFT methodologies.[46] Therefore, CASSCF/CASPT2 excitation energies will be used as a reference. The active space is constituted by 4π and $4\pi^*$ valence molecular orbitals (8 MOs) and 8 electrons. A systematic study using an increasing active space composed of $n\pi/n\pi^*$ ($n = 1−6$) MOs and their corresponding housed electrons was in fact performed, and the convergence of the excitation energies was already achieved

at the $4\pi/4\pi^*$ level. The CASSCF state-interaction (CASSI) method was employed to compute the oscillator strength with the CASPT2 excitation energies.[70,71] CASSCF/CASPT2 calculations were carried out with the MOLCAS 7.2 package.[72]

CT excitation energies were then calculated using standard TD-DFT methodology and the B3LYP, BHHLYP, B2PLYP, M06-2X, and M06-HF functionals. CT excitations were also evaluated using LC functionals as Coulomb-attenuaded CAM-B3LYP,[49] LC-wPBE,[48] and wB97X-D. The excitation energies for B2PLYP were computed according to the Neese and Grimme procedure.[54] In this procedure and in complete analogy to the ground-state treatment, a scaled second-order perturbation correction to configuration interaction with singles (CIS(D)) wave functions developed some years ago by Head-Gordon et al.[73] is computed on the basis of density functional data and added to the TD-DFT excitation energies as follows:

$$\omega_{corr} = \omega_{TD-B2PLYP} + a_c \Delta_{(D)} \qquad (4)$$

where ω_{corr} is the corrected excitation energy, $\omega_{TD-B2PLYP}$ is the TD-B2PLYP excitation energy computed in a standard way and $\Delta_{(D)}$ is the second-order perturbation term. The a_c parameter is equal to that used for the ground state. B2PLYP calculations were done using ORCA, whereas the rest of TD-DFT calculations used Gaussian 09. Vertical CT excitation energies were computed using the cc-pVDZ basis set.

RESULTS AND DISCUSSION

Intermolecular Interaction Energies. As previously discussed, the description of the ground-state potential energy curves of the 3T−TCNQ complex requires accurate quantum chemical calculations fully accounting for $\pi−\pi$ stacking interactions. Figure 2 displays the potential energy curves calculated for the cofacial 3T−TCNQ complex at the SCS-MP2/cc-pVTZ level (taken here as a reference) and at the DFT level using different functionals in combination with the cc-pVDZ basis set. The potential energy curves in Figure 2 are computed without taking into account the BSSE correction. The importance of the
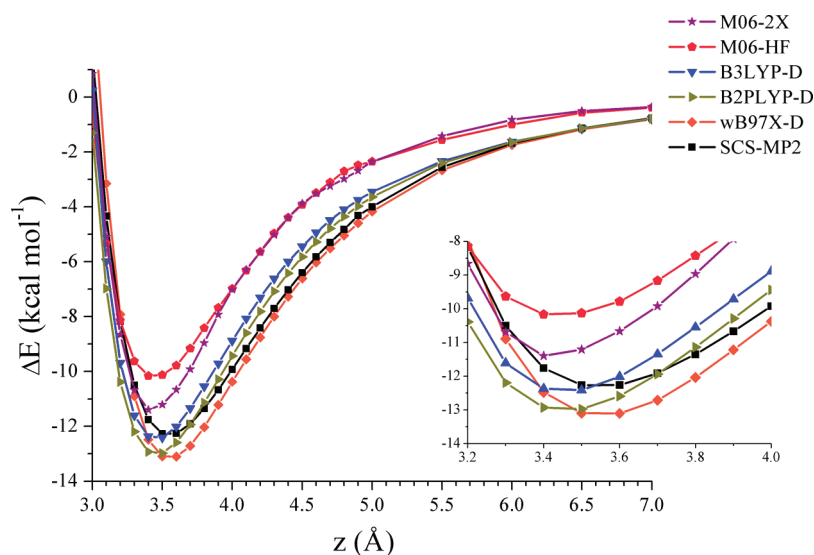
Figure 3. Potential energy curves for the cofacial 3T−TCNQ complex computed at various DFT levels with the cc-pVTZ basis set. The SCS-MP2/cc-pVTZ curve is shown as a reference. All intermolecular interaction energies (ΔE) are corrected for BSSEs by the counterpoise technique.

BSSE correction and of the size of the basis set employed with DFT calculations is later analyzed. SCS-MP2 calculations predict a minimum of −15.97 kcal mol^{-1} at a separation of 3.44 Å between the molecular planes. Note that SCS-MP2 calculations provide a significant improvement with respect to MP2, as reported before for related D−A complexes.[74]

The potential energy curves provided by DFT methods can be interpreted according to the nature of the functional employed (Figure 2). As expected, the hybrid B3LYP and BHHLYP functionals predict too shallow potential energy curves with energy minima of −1.23 and −2.41 kcal mol^{-1}, respectively, and thus dramatically underestimate the interaction energies compared to SCS-MP2/cc-pVTZ results. The optimum intermolecular distances (B3LYP: 4.15 Å, BHHLYP: 3.94 Å) are strongly overestimated in comparison with that obtained at the SCS-MP2 level (3.44 Å) and with those commonly found for related $\pi-\pi$ complexes (3.4−3.5 Å).[75] Though they predict a bound dimer, the hybrid functionals do not therefore properly account for $\pi-\pi$ stacking interactions in the 3T−TCNQ complex, as previously reported for similar $\pi-\pi$ complexes.[75,76] The culprit for the rather unsatisfactory performance of the hybrid functionals in describing intermolecular interactions is the local nature of the correlation kernel. Therefore, in hybrid functionals the correlation energy is calculated only from the local properties of the density, and the dispersion energy, which arises from a truly nonlocal correlation effect, cannot be explicitly described.

The double hybrid B2PLYP functional partially accounts for the dispersion energy. This effect is clearly observed in the potential energy curve computed for the 3T−TCNQ complex, which exhibits a deeper energy minimum (−6.27 kcal mol^{-1}) compared to B3LYP and BHHLYP results. The minimum-energy intermolecular distance is 3.63 Å, in better agreement with that obtained at the SCS-MP2 level (3.44 Å). The better description of the dispersion energy provided by B2PLYP arises from the incorporation of dynamical electron correlation effects through a perturbative second-order correlation term obtained from the KS orbitals and eigenvalues.[62] Despite the partial introduction of nonlocal electron correlation effects,

the interaction energy predicted by B2PLYP in the minimum-energy region underestimates by ∼10.0 kcal mol^{-1} the SCS-MP2 value.

In order to obtain more accurate potential energy curves, DFT calculations using hybrid meta functionals (M06-2X and M06-HF) and incorporating a dispersion term (DFT-D) were carried out. The M06-2X and M06-HF functionals yield quantitatively reliable potential energy curves with potential energy minima of −14.96 and −15.90 kcal mol^{-1}, respectively. The minimum-energy intermolecular separations are predicted at 3.40 and 3.39 Å, respectively, which are slightly shorter than that estimated at the SCS-MP2 level. Both the interaction energies and the intermolecular distances are in good agreement with the SCS-MP2 results. However, the curves generated using these functionals are narrower than that predicted at the SCS-MP2 level. The addition of the dispersion correction term to the B3LYP, B2PLYP, and wB97X functionals, denoted as B3LYP-D, B2PLYP-D, and wB97X-D, gives rise to a fully quantitative description of the potential energy curve. The three DFT-D functionals predict interaction energies at the minimum (−14.84, −14.72, and −16.14 kcal mol^{-1} for B3LYP-D, B2PLYP-D, and wB97X-D, respectively) very close to that computed at the SCS-MP2 level (−15.97 kcal mol^{-1}) with differences of ∼1 kcal mol^{-1}. The optimum 3T−TCNQ intermolecular distances are calculated at 3.39 (B3LYP-D), 3.39 (B2PLYP-D), and 3.49 Å (wB97X-D), slightly underestimating (B3LYP-D and B2PLYP-D) and overestimating (wB97X-D) the SCS-MP2 value (3.44 Å). Among the hybrid meta and the DFT-D functionals employed to describe the 3T−TCNQ complex, the wB97X-D seems to yield the best performance to estimate the potential energy curve (see Figure 2).

In a further step, the potential energy curves for the cofacial 3T−TCNQ complex were recalculated including BSSE corrections and the larger cc-pVTZ basis set (Figure 3). As a consequence of BSSE corrections, the depth of the well for the SCS-MP2 curve decreases ∼4 kcal mol^{-1} and the minimum-energy intermolecular distance undergoes a significant increase going from 3.44 to 3.55 Å. The potential energy minimum is now predicted at −12.31 kcal mol^{-1}.
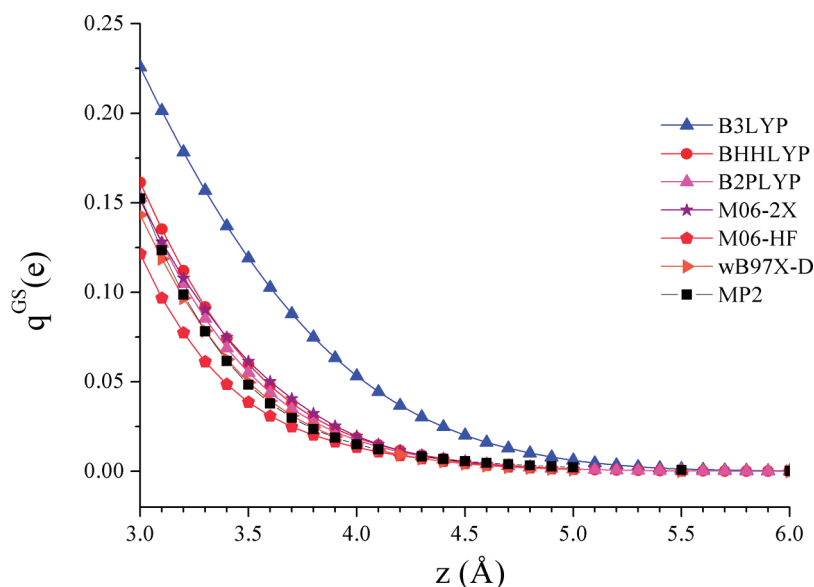
Figure 4. Mulliken charge transferred from 3T to TCNQ in the ground state (q^{GS}) calculated with different functionals as a function of the intermolecular distance (z) in the cofacial geometry.

A detailed inspection of Figure 3 reveals that DFT-D functionals (B3LYP-D, B2PLYP, and wB97X-D) yield potential energy curves that are better than those obtained by M06 functionals (M06-2X and M06-HF). The M06-2X and M06-HF functionals underestimate by more than 1 kcal mol^{-1} the intermolecular interaction energies at the minimum-energy region. The optimum intermolecular distances are found at 3.41 and 3.43 Å, respectively, which are too short compared to the SCS-MP2 value (3.55 Å). It should be noted that at longer distances, the potential energy curve produced by M06-2X deviates significantly from the SCS-MP2 curve (and the DFT-D curves), with energies that rise sharply in the range between the minimum and 4.0 Å. As a consequence, the M06-2X potential well is too narrow near the minimum. The DFT-D functionals predict interaction energies at the minimum (-12.46, -13.02, and -13.16 kcal mol^{-1} for B3LYP-D, B2PLYP-D, and wB97X-D, respectively), very close to that computed at the SCS-MP2 level (-12.31 kcal mol^{-1}). In terms of minimum-energy intermolecular separations, wB97X-D gives the best result, with a potential energy minimum placed at 3.56 Å, which matches perfectly with that calculated at the SCS-MP2 level. The intermolecular distance afforded by B3LYP-D and B2PLYP-D functionals (3.45 Å) underestimates the SCS-MP2 value by ~0.1 Å. It is worth to note that both B3LYP-D and wB97X-D functionals in conjunction with the cc-pVTZ basis set result in small BSSEs of ~1 kcal mol^{-1} (Figure S1, Supporting Information).

The results clearly point out that DFT-D functionals in combination with cc-pVTZ basis set yield the best performance to estimate the potential energy curves for the 3T−TCNQ complex. Among them, wB97X-D predicts accurate interaction energies and yields the best intermolecular distances. In addition to the dispersion term, the wB97X-D functional is built on the basis of the long-range corrected scheme which already partially takes noncovalent interactions into account.[51] The LC scheme seems to be important not only for the treatment of noncovalent interactions but also for the description of CT excited states, as will be discussed below. It is also important to stress that wB97X-D in combination with the cc-pVDZ basis set and without

correction of the BSSE, although overestimates the interaction energies by about 4 kcal mol^{-1}, is able to provide relatively accurate intermolecular distances. This information is of great relevance in order to study larger $\pi-\pi$ D−A complexes for which more extended basis sets are prohibitive.

Ground-State Charge-Transfer Analysis. $\pi-\pi$ D−A molecular complexes are characterized by a small amount of charge transferred from the donor to the acceptor in the ground state.[77] Unfortunately, the charge distribution calculated for the 3T−TCNQ complex in the ground state strongly relies on the choice of the functional. Figure 4 shows the evolution of the Mulliken charge transferred from 3T to TCNQ in the cofacial configuration as a function of the intermolecular distance. To test the reliability of the Mulliken charges, the charge transferred from 3T to TCNQ was also analyzed according to the CHelpG scheme (Figure S2, Supporting Information).[78] The charges obtained from this scheme are similar to those computed using the Mulliken approach, and therefore, Mulliken charges will be used in the following discussion. It should be mentioned that Hobza et al. have recently shown that Mulliken analysis lead to reliable estimates of the charge transferred in a family of D−A complexes.[79]

The amount of charge decays quickly with increasing separation between the 3T and TCNQ molecules (Figure 4). Although all functionals display this behavior, B3LYP clearly tends to overestimate the charge transferred in the ground state. For instance, at an intermolecular distance of 3.4 Å in the minimum-energy region, B3LYP predicts a CT of 0.14e, whereas BHHLYP, B2PLYP, and M06-2X yield a value of ~0.07e, and wB97X-D, M06-HF, and MP2[80] lead to charge transfers smaller than 0.07e. These results corroborate that increasing the percentage of HF exchange in the functional causes a decrease of the amount of charge transferred in the ground state of the 3T−TCNQ complex. This trend is in agreement with recent results reported for the tetrathiafulvalene−TCNQ D−A complex.[74] Therefore, the choice of standard hybrid functionals, such as B3LYP, for studying D−A complexes should be taken with care, since the amount of charge transferred in the ground state is artificially
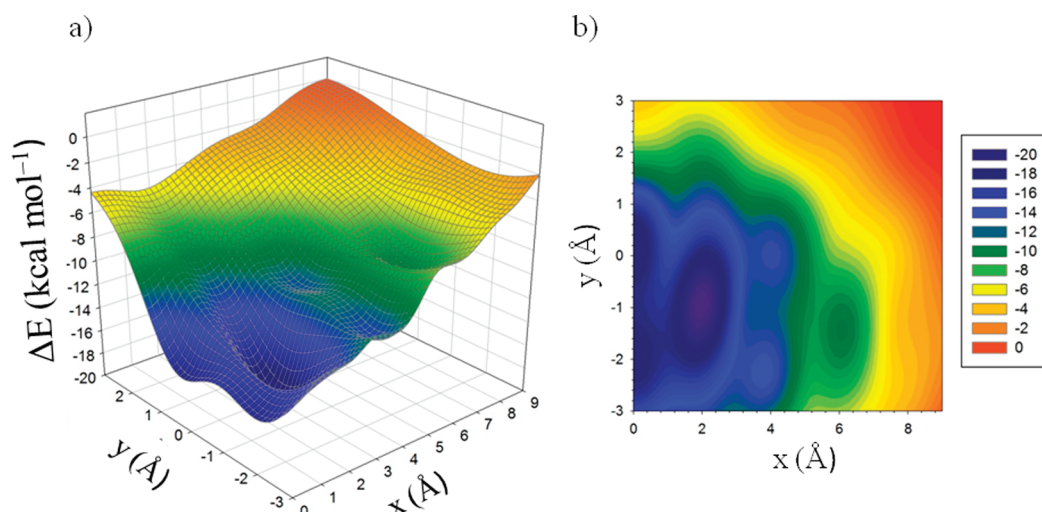
Figure 5. (a) Potential energy surface computed at the B3LYP-D/cc-pVDZ level for the 3T−TCNQ complex at a fixed intermolecular distance (z) of 3.39 Å. (b) Interaction energy contour map (kcal mol^{-1}).

Table 1. Optimized Geometries of the Three Most Stable Structures (1−3) Calculated for the 3T−TCNQ Complex[a]

distances	B3LYP-D		wB97X-D	
	cc-pVDZ	cc-pVTZ	cc-pVDZ	cc-pVTZ
a	3.170	3.177	3.307	3.310
b	3.170	3.177	3.307	3.311
c	3.136	3.175	3.278	3.325
d	3.205	3.228	3.343	3.373
e	3.240	3.264	3.349	3.385
f	3.120	3.145	3.296	3.344
g	3.043	3.063	3.192	3.221
h	3.224	3.250	3.371	3.404
i	3.220	3.250	3.370	3.404
j	3.041	3.064	3.192	3.220

[a] The shortest carbon−carbon intermolecular distances (in Å) are given.

high, and it can even increase upon full geometry optimization, as will be discussed next.

Optimized Geometries. With the aim of identifying the most stable structures of the 3T−TCNQ complex, a comprehensive exploration of the energy landscape along the x and y axis (see Figure 1) is required. Figure 5 depicts the potential energy surface and its respective contour map computed at the B3LYP-D/cc-pVDZ level by varying the distance along the x and y axis and by maintaining the monomers frozen at the minimum-energy intermolecular distance ($z = 3.39$ Å). The most stable structures are located in the dark-blue region of the potential energy surface. Three minimum-energy conformations were found and used subsequently as starting points for full geometry optimizations at B3LYP-D and wB97X-D levels in conjunction with cc-pVDZ and cc-pVTZ basis sets.

Geometry optimizations lead to the three minimum-energy structures (1−3) depicted in Table 1. Structures **1** and **3** differ

only in the relative displacement of the monomers along the short molecular y axis. In structure **1**, the benzene ring of TCNQ is centered above the single C_β−C_β bond of the central thiophene ring of 3T, whereas in **3** the midpoint of the benzene ring is approximately placed above the central sulfur atom of 3T. In contrast, TCNQ in structure **2** is mainly displaced along the long molecular x-axis, and the benzene ring is now located above one of the inter-ring C_α−$C_{\alpha'}$ bonds of 3T. Geometry optimizations using cc-pVTZ provide structures almost identical to those obtained with cc-pVDZ, but with a much higher computational cost. The optimized intermolecular distances differ by less than 0.01 Å for structure **1** and by ∼0.03 Å in structures **2** and **3** (Table 1). Although both B3LYP-D and wB97X-D functionals give rise to minimum-energy structures with identical orientations, it is noteworthy that they predict different intermolecular distances. The closest carbon−carbon intermolecular distances found at the B3LYP-D level are in the 3.0−3.2 Å range. Such values are considerably shorter than those computed at the CCSD(T) level for a benzene−hexafluorobenzene complex (3.5−3.6 Å).[81] In contrast, wB97X-D leads to a larger separation between the interacting molecules with carbon−carbon distances ranging from 3.2 to 3.4 Å. Therefore, wB97X-D provides more reliable intermolecular distances than those obtained with B3LYP-D.

Table 2 collects the interaction energies computed by performing single-point calculations using the cc-pVTZ basis set and the fully relaxed cc-pVDZ geometries. Calculations using the cc-pVTZ optimized geometries lead to interaction energies that differ from those in Table 2 by less than 0.1 kcal mol^{-1} (Table S1, Supporting Information). Calculations therefore show that the small structural changes found in passing from cc-pVDZ to cc-pVTZ optimized structures have no significant effect on the interaction energies and that cc-pVDZ optimized geometries can be safely used to calculate the interaction energies. This is of special interest when dealing with larger D−A complexes for which geometry optimizations using the cc-pVTZ basis set would be computationally prohibitive.

The CP-corrected interaction energies clearly indicate that structure **2** is the most stable with binding energies of −20.32 and −17.78 kcal mol^{-1} at B3LYP-D and wB97X-D levels,

Table 2. Interaction Energies (kcal mol^{-1}) Calculated for the Most Stable Structures of the 3T−TCNQ Complex^a

method	1	2	3
B3LYP-D/cc-pVTZ^b	−15.87 (−17.00)	−20.32 (−21.60)	−16.83 (−18.03)
SCS-MP2/cc-pVTZ^b	−14.03 (−18.90)	−17.28 (−22.78)	−14.83 (−19.84)
wB97X-D/cc-pVTZ^c	−14.88 (−15.85)	−17.78 (−18.86)	−15.66 (−16.65)
SCS-MP2/cc-pVTZ^c	−13.95 (−18.14)	−16.65 (−21.33)	−14.62 (−18.86)

^{a} Energies are corrected for BSSE using the counterpoise method (counterpoise uncorrected values are given within parentheses). ^{b} Single-point energy calculations on the B3LYP-D/cc-pVDZ optimized geometries. ^{c} Single-point energy calculations on the wB97X-D/cc-pVDZ optimized geometries.
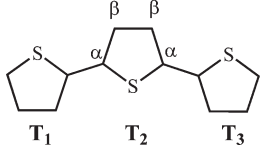
respectively. Although the absolute difference between the interaction energies calculated for structures **1** and **3** using B3LYP-D and wB97X-D is almost constant (∼1 kcal mol^{-1}), the relative energies of the three conformers vary with the functional. More specifically, **1** and **3** lie 4.45 and 3.49 kcal mol^{-1} above **2** at the B3LYP-D level, whereas they are found 2.90 and 2.12 kcal mol^{-1} higher in energy than **2** at the wB97X-D level. This arises because B3LYP-D stabilizes considerably **2** compared to wB97X-D results (see Table 2). It is interesting to note that both B3LYP-D and wB97X-D slightly overestimate the binding energies of the three minimum-energy structures when compared to SCS-MP2 energies. However, wB97X-D yields interaction energies that are closer to those obtained at SCS-MP2 level with differences around 1 kcal mol^{-1}.

Table 2 reveals that DFT-D and SCS-MP2 methods present significantly different BSSEs. B3LYP-D gives rise to errors in the 1.12−1.29 kcal mol^{-1} range, whereas wB97X-D yields errors which range from 0.98 to 1.08 kcal mol^{-1}. The slightly smaller BSSEs found for wB97X-D are likely due to the fact that wB97X-D-optimized structures show longer intermolecular distances than B3LYP-D structures. SCS-MP2/cc-pVTZ interaction energies show the largest BSSEs, with values around 4.8 kcal mol^{-1} for the three minimum-energy structures. These results contrast to those reported for relevant biological complexes, where SCS-MP2/cc-pVTZ was found to be almost free from BSSE due to error compensations.[21] Our results therefore point to the importance of including BSSE corrections at the SCS-MP2 level to compute accurate interaction energies in D−A conjugated complexes as 3T−TCNQ. In contrast, DFT-D methods in combination with cc-pVTZ basis sets lead to rather small BSSEs.

Full geometry optimizations allow for a careful analysis of the changes occurred in the 3T and TCNQ monomers upon formation of the complex. The structural changes can be easily quantified by using the carbon−carbon single−double bond length alternation (BLA), which estimates the degree of aromatization/quinoidization along the conjugated backbone.[82] The BLA parameter has been widely used to characterize the carbon skeleton in different families of oligothiophenes[83−85] and is calculated for each thiophene ring as the difference between the length of the C_β−C_β bond and the average of the two C_α−C_β bonds (see sketch in Table 2). An aromatic ring is thus characterized by a positive BLA value, while a quinoid ring shows a negative BLA value.

Table 3 gathers the BLA values for 3T and the Mulliken charge transferred from 3T to TCNQ (q^{GS}) computed for structure **2** at the B3LYP-D/cc-pVDZ and wB97X-D/cc-pVDZ levels. The use of the cc-pVTZ basis set has almost no effect on the BLA values, and the charge distribution (Table S2). BLA data for isolated 3T are also included in Table 3 for comparison. At the B3LYP-D

Table 3. Bond Length Alternation Values (in Å) Computed at the B3LYP-D/cc-pVDZ and wB97X-D/cc-pVDZ Levels for Each Thiophene Ring of 3T in Structure 2 and for Isolated 3T^a

3T	T_1	T_2^{b}	T_3^{b}	q^{GS}(e)
		B3LYP-D		
isolated	0.047	0.036	0.047	−
2	0.041	0.012	0.030	0.30
		wB97X-D		
isolated	0.056	0.047	0.056	−
2	0.052	0.038	0.046	0.12

^{a} The Mulliken charge transferred from 3T to TCNQ (q^{GS}) is also included. ^{b} TCNQ lies on top of the T_2 and T_3 thiophene rings, as illustrated in Table 1.

level, the BLA values computed for 3T in the complex are significantly smaller than those of isolated 3T. For instance, the BLA obtained for the central ring (T_2) decreases from 0.036 Å in isolated 3T to 0.012 Å in the complex. The reduction of BLA for the thiophene spine in the 3T−TCNQ complex indicates a loss of aromatic character of the conjugated backbone compared to isolated 3T. The partial quinoidization of 3T results from the charge transferred from 3T to TCNQ (0.30e, Table 2). In oligothiophenes, quinoidization of the carbon skeleton is produced upon injection of charges in oxidation/reduction processes.[84]

In contrast to B3LYP-D, wB97X-D predicts more localized structures with larger BLA values, owing to the higher amount of HF-like exchange included in this functional. This behavior has been previously reported for related conjugated systems.[86] The comparison between the BLA values computed at the wB97X-D level for isolated 3T and for 3T in structure **2** reveals less marked differences than those obtained at the B3LYP-D level (Table 2). The less pronounced structural relaxation calculated for 3T at the wB97X-D level matches perfectly with the smaller amount of charge transferred (0.12e) from 3T to TCNQ.

Calculations therefore show that the B3LYP-D functional overestimates the charge transfer between the donor and the acceptor in the D−A complex. This leads to too short intermolecular distances and to too large changes on the structures of the monomers when the geometry of the complex is fully relaxed. The wB97X-D functional provides more accurate intermolecular distances and predicts smaller structural changes on the monomers forming the complex, due to the lower charge transfer, which is in better agreement with the description expected for weakly interacting D−A complexes.

Charge-Transfer Excited States. The characterization of CT excited states in D−A complexes is of utmost importance to understand the photophysical properties of these complexes and their potential use in organic solar cells. In order to gain insight into the performance of several functionals to treat CT excitations, the excitation energies of the lowest CT state were computed using the TD-DFT approach and the optimized ground-state molecular geometries of structures **1**−**3**. Hybrid (B3LYP, BHHLYP), hybrid meta (M06-2X, M06-HF), double-hybrid (B2PLYP),
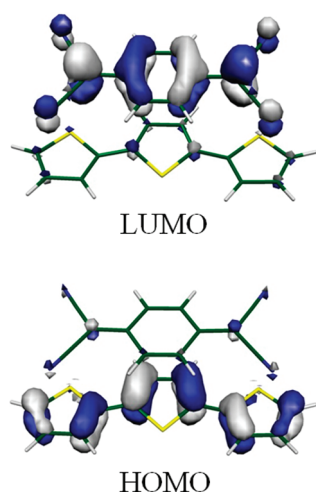
2074

dx.doi.org/10.1021/ct200203k |J. Chem. Theory Comput. 2011, 7, 2068–2077

LUMO

HOMO

Figure 6. Electronic density isocontours $(0.03 \text{ e bohr}^{-3})$ calculated at the CASSCF level for the frontier molecular orbitals of the 3T−TCNQ complex.

and LC-corrected (CAM-B3LYP, wB97X-D, LC-wPBE) functionals have been chosen for TD-DFT calculations. CASSCF/CASPT2 calculations have been carried out to benchmark the TD-DFT results. Figure 6 depicts the topologies of selected molecular orbitals as a guide to the description of the lowest CT excitation. Table 4 collects CT excitation energies and oscillator strengths computed using TD-DFT and CASPT2 methodologies.

According to the CASPT2 calculations, the lowest singlet excited state (S_1) is computed at 1.79, 1.72, and 1.83 eV above the ground state (S_0) for **1**−**3**, respectively (Table 4). The intensity of the $S_0{\rightarrow}S_1$ transition clearly depends on the configuration of the complex, with oscillator strength values of $f = 0.044$ for **1**, $f = 0.176$ for **2**, and $f = 0.059$ for **3**. For the three structures, the CASSCF wave function is dominated by the promotion of an electron from the highest occupied molecular orbital (HOMO) to the lowest unoccupied molecular orbital (LUMO). The HOMO is completely localized on the conjugated carbon−carbon skeleton of 3T, whereas the LUMO is located on the conjugated backbone of TCNQ (see Figure 6). Therefore, the $S_0{\rightarrow}S_1$ transition corresponds to a CT excitation and is proposed to be responsible for the weak feature detected experimentally at 1.49 eV in chloroform.[12]

Note that CASPT2 calculations are performed in gas-phase while the experimental data are recorded in solution. Stein et al.[87] recently studied a family of aromatic donor−tetracyanoethylene complexes, for which optical data in gas phase and solution are available, and concluded that solvent models hardly stabilize the lowest CT states and are not able to reproduce the experimental solvent effect that lowers the CT excitation energies by 0.32 eV on average. These authors suggest that the only reasonable way to proceed in these cases is to assume that subtraction of 0.32 eV from the gas phase calculations makes them comparable to experiments in solvent. Using this assumption, the CASPT2 results match now perfectly the experimental CT excitation found at 1.49 eV for the 3T−TCNQ complex. Hence, the CASPT2 gas-phase energies can be reasonably employed to benchmark the TD-DFT results.

As can be seen in Table 4, all functionals predict larger CT excitation energies for structure **2** than for **1** and **3**, which contrasts to CASPT2 results. Concerning the intensities, all

Table 4. $S_0{\rightarrow}S_1$ Vertical Excitation Energies (eV) Computed for Structures 1−3 of the 3T−TCNQ Complex

method[a]	**1**[b]	**2**[b]	**3**[b]
CASPT2	1.79 (*0.044*)	1.72 (*0.176*)	1.83 (*0.059*)
B3LYP	1.25 (*0.070*)	1.46 (*0.112*)	1.32 (*0.075*)
BHHLYP	1.71 (*0.067*)	1.88 (*0.121*)	1.72 (*0.060*)
B2PLYP	1.30 (*0.060*)	1.48 (*0.115*)	1.29 (*0.053*)
M06-2X	1.73 (*0.062*)	1.89 (*0.109*)	1.73 (*0.053*)
M06-HF	2.63 (*0.062*)	2.68 (*0.125*)	2.65 (*0.053*)
LC-wPBE	2.49 (*0.055*)	2.54 (*0.111*)	2.52 (*0.045*)
CAM-B3LYP	1.75 (*0.063*)	1.91 (*0.114*)	1.76 (*0.055*)
wB97X-D	1.81(*0.062*)	1.96 (*0.115*)	1.83 (*0.055*)

[a] All calculations were performed with the cc-pVDZ basis set. [b] Oscillator strength (*f*) values are given within parentheses.

functionals predict the highest oscillator strength for structure **2** in good agreement with CASPT2 oscillator strengths. CT excitation energies using the TD-DFT approach are analyzed according to the nature of the functional (hybrid, double hybrid, hybrid meta, and long-range functionals) and the amount of HF-like exchange. B3LYP, which incorporates a small percentage (20%) of HF-like exchange, underestimates the CASPT2 CT excitation energies with deviations of up to −0.54 eV. In contrast, the CT excitations computed by BHHLYP (50% of HF-like exchange) yield CT excitation energies closer to those computed at the CASPT2 level. The largest deviation is found for structure **2**, for which the CT state is calculated 0.16 eV higher in energy.

The double-hybrid B2PLYP functional also underestimates the CT excitation energies with deviations from −0.24 (**2**) to −0.54 eV (**3**). The underestimation of the CT excitations results from the perturbative correction term $(\Delta_{(D)})$ computed through the CIS(D) method (see Theoretical and Computational Details Section) that stabilizes the CT state. Note that B2PLYP has a 53% of HF-like exchange, and thus, when the $\Delta_{(D)}$ term is not added, the uncorrected CT excitation energies are similar to those computed at BHHLYP level.

The hybrid meta M06-2X functional predicts CT excitation energies with accuracy similar to that obtained at BHHLYP level (Table 4). The resemblance in the CT excitation energies is due to the fact that M06-2X incorporates a 54% of HF-like exchange very close to the 50% included in BHHLYP. In contrast, M06-HF implies a 100% of HF-like exchange and dramatically overestimates the CT excitation energies with a deviation of up to 0.96 eV with respect to CASPT2 values. These results are consistent with those recently reported by Li et al. showing that for CT transitions at intermediate interelectronic separations M06-2X performs notably, whereas M06-HF fails completely.[88]

LC-wPBE, CAM-B3LYP, and wB97X-D represent a more sophisticated class of functionals based on the long-range corrected scheme. However, the behavior of LC-wPBE is quite different with respect to their homologous CAM-B3LYP and wB97X-D due to the amount of HF-like exchange. LC-wPBE has a 0% of HF-like exchange at short-range and a 100% at long-range and overestimates severely the CT excitation energies with deviations ranging from 0.69 to 0.80 eV compared to that of the CASPT2 results. CAM-B3LYP shows a 19 and 65% of HF-like exchange at short and long interelectronic separations, whereas wB97X-D includes a 22 and 100%, respectively. Both funtionals predict similar CT excitation energies, the largest deviation being found for structure **2** with differences of 0.19 and 0.24 eV for

CAM-B3LYP and wB97X-D, respectively. wB97X-D performs slightly better than CAM-B3LYP for structures **1** and **3**, for which it provides CT excitations in excellent accord with CASPT2 data.

Overall, wB97X-D provides the best performance with the smallest deviations in the CT excitation energies in comparison to CASPT2 results, although CAM-B3LYP, BHHLYP, and M06-2X functionals also behave accurately enough. The results evidence that the CT transition in the 3T−TCNQ complex occurs at intermediate interelectronic separations, and thus, not only long-range corrected functionals describe correctly this transition but also hybrid and hybrid meta functionals with an appropriate portion of HF-like exchange. It should be also mentioned that the size of the basis set has no special effect on the CT excitation energies. For instance, almost identical excitation energies are obtained at wB97X-D/cc-pVDZ (1.96 eV) and wB97X-D/cc-pVTZ (1.98 eV) levels for structure **2**.

■ CONCLUSIONS

We have presented a detailed quantum chemical investigation of the terthiophene−tetracyanoquinodimethane complex as model for $\pi-\pi$ D−A systems. The study has focused on the performance of several functionals to treat $\pi-\pi$ intermolecular interactions, the distribution of charge in the ground state of the complex, the identification and the characterization of the most stable supramolecular structures, and the description of the CT excitation found in these D−A complexes.

Density functionals including the dispersion term (DFT-D) treat in an accurate way the $\pi-\pi$ interactions yielding potential energy curves similar to those computed at the SCS-MP2 level. The distribution of the charge in the ground state is clearly determined by the portion of HF-like exchange in the functional. The charge transferred from the donor to the acceptor in the ground state is inversely proportional to the percentage of HF-like exchange. Hence, a too large charge transfer is predicted when using the common B3LYP functional. When characterizing the most stable structures of the complex, wB97X-D functional predicts reliable intermolecular distances, small structural changes in the monomers forming the complex, and a small amount of charge transferred from 3T to TCNQ in the ground state, in agreement with the chemically intuitive description of weak interacting D−A complexes. High-level ab initio CASSCF/CASPT2 calculations have enabled to benchmark the TD-DFT results for excited states. Long-range corrected functionals, such as CAM-B3LYP and wB97X-D, as well as the hybrid BHHLYP are able to treat accurately the CT excitations for the 3T−TCNQ complex, yielding values very similar to those obtained by the CASPT2 method.

Overall, the wB97X-D functional displays the best performance to treat $\pi-\pi$ intermolecular interactions and CT excitations in a balanced way, for the 3T−TCNQ complex, thanks to the combination of dispersion and long-range corrected terms. Hence, the wB97X-D functional might be reliably used to further investigate $\pi-\pi$ D−A complexes. Calculations show that the use of a cc-pVTZ basis set is needed to predict accurate interaction energies with small BSSEs, whereas reliable optimized geometries and excitation energies are obtained using the less-demanding cc-pVDZ basis set. Theoretical information for larger D−A complexes would be very useful to guide experimentalists in the design of fine-tuned D−A complexes for organic solar cells.

■ ASSOCIATED CONTENT

ⓢ Supporting Information. B3LYP-D/cc-pVTZ and wB9-7X-D/cc-pVTZ counterpoise corrected and uncorrected potential energy curves; CHelpG charge transferred from 3T to TCNQ as a function of the functional and the intermolecular distance; B3LYP-D/cc-pVTZ and wB97X-D/cc-pVTZ interaction energies as a function of the optimization level; and influence of the basis set on BLA and charge transferred. This material is available free of charge via the Internet at http://pubs.acs.org.

■ AUTHOR INFORMATION

Corresponding Author
*E-mail: enrique.orti@uv.es.

■ ACKNOWLEDGMENT

■ REFERENCES

(1) Sariciftci, N. S.; Smilowitz, L.; Heeger, A. J.; Wudl, F. *Science* **1992**, *258*, 1474.

(2) Schmidt-Mende, L.; Fechtenkotter, A.; Mullen, K.; Moons, E.; Friend, R. H.; MacKenzie, J. D. *Science* **2001**, *293*, 1119.

(3) Brédas, J. L.; Norton, J. E.; Cornil, J.; Coropceanu, V. *Acc. Chem. Res.* **2009**, *42*, 1691.

(4) Dimitrakopolous, C. D.; Malefant, P. *Adv. Mater.* **2002**, *14*, 99.

(5) Murphy, A. R.; Fréchet, J. M. J. *Chem. Rev.* **2007**, *107*, 1066.

(6) Mishra, A.; Ma, C.-Q.; Baüerle, P. *Chem. Rev.* **2009**, *109*, 1141.

(7) Perepichka, I. F.; Perepichka, D. F. *Handbook of Thiophene-Based Materials: Applications in Organic Electronics and Photonics*; Wiley: Weinheim, Germany, 2009.

(8) Ferraris, J.; Cowan, D. O.; Walatka, V.; Perlstein, J. H. *J. Am. Chem. Soc.* **1973**, *95*, 948.

(9) Coleman, L. B.; Cohen, M. J.; Sandman, D. J.; Yamaguchi, F. G.; Garito, A. F.; Heeger, A. J. *Solid State Commun.* **1973**, *12*, 1125.

(10) Aziz, E. F.; Vollmer, A.; Eisebitt, S.; Eberhardt, W.; Pingel, P.; Neher, D.; Koch, N. *Adv. Mater.* **2007**, *19*, 3257.

(11) Braun, K.-F.; Hla, S. W. *J. Chem. Phys.* **2008**, *129*, 064707.

(12) Panda, P.; Veldman, D.; Sweelssen, J.; Bastiaansen, J. J. A. M.; Langeveld-Voss, B. M. W.; Meskers, S. C. J. *J. Phys. Chem. B* **2007**, *111*, 5076.

(13) Stone, A. J. *The Theory of Intermolecular Forces*; Oxford University Press: Oxford, U.K., 1997.

(14) Pitonak, M.; Riley, K. E.; Neogrady, P.; Hobza, P. *Phys. Chem. Chem. Phys.* **2008**, *9*, 1636.

(15) Sinnkrot, M. O.; Sherrill, C. D. *J. Phys. Chem. A* **2004**, *108*, 10200.

(16) Cremer, D. *Encyclopedia of Computational Chemistry*; P. v. R. Schleyer, Ed.; Wiley: New York, 1998; Vol.3, p 1706.

(17) Hobza, P.; Selzle, H. L.; Schkag, E. W. *J. Chem. Phys.* **1996**, *100*, 18790.

(18) Sinnkrot, M. O.; Valeev, E. F.; Sherrill, C. D. *J. Am. Chem. Soc.* **2002**, *124*, 10887.

(19) Tsuzuki, S.; Honda, K.; Uchimaru, T.; Mikami, M. *J. Chem. Phys.* **2004**, *120*, 647.

(20) Grimme, S. *J. Chem. Phys.* **2003**, *118*, 9095.

(21) Antony, J.; Grimme, S. *J. Phys. Chem. A* **2007**, *111*, 4862.

(22) Kristyan, S.; Pulay, P. *Chem. Phys. Lett.* **1994**, *229*, 175.

(23) Hobza, P.; Sponer, J.; Reschel, T. J. *J. Comput. Chem.* **1995**, *11*, 1315.

(24) Allen, M.; Tozer, D. J. *J. Chem. Phys.* **2002**, *117*, 11113.

(25) Dion, M.; Rydberg, H.; Scroder, E.; Langreth, D. C.; Lundqvist, B. I. *Phys. Rev. Lett.* **2004**, *92*, 246401.

(26) Lee, K.; Murray, E. D.; Kong, L.; Lundqvist, B. I.; Langreth, D. C. *Phys. Rev. B* **2010**, *82*, 081101.

(27) Cooper, V. R. *Phys. Rev. B* **2010**, *81*, 161104.

(28) Vydrov, O. A.; Van Voorhis, T. *J. Chem. Phys.* **2010**, *132*, 164113.

(29) Vydrov, O. A.; Van Voorhis, T. *J. Chem. Phys.* **2010**, *133*, 244103.

(30) Becke, A. D.; Johnson, E. R. *J. Chem. Phys.* **2007**, *127*, 154108.

(31) Román-Pérez, G.; Soler, J. M. *Phys. Rev. Lett.* **2009**, *103*, 096102.

(32) Heβelmann, A.; Jansen, G.; Schütz, M. *J. Chem. Phys.* **2005**, *122*, 14103.

(33) Zhao, Y.; Truhlar, D. G. *J. Phys. Chem.* **2006**, *125*, 194101.

(34) Zhao, Y.; Truhlar, D. G. *Theor. Chem. Acc.* **2008**, *120*, 215.

(35) Elstner, M.; Hobza, P.; Suhai, S.; Kaxiras, E. *J. Chem. Phys.* **2001**, *114*, 5149.

(36) Wu, Q.; Yang, W. *J. Chem. Phys.* **2002**, *115*, 515.

(37) Zimmerli, U.; Parrinello, M.; Koumoutsakos, P. *J. Chem. Phys.* **2004**, *120*, 5149.

(38) Grimme, S. *J. Comput. Chem.* **2004**, *25*, 1463.

(39) Grimme, S. *J. Comput. Chem.* **2006**, *27*, 1787.

(40) Ducere, J.-M.; Cavallo, L. *J. Phys. Chem. B* **2007**, *111*, 13124.

(41) Tapavicza, E.; Lin, I.-C.; von Lilienfeld, O. A.; Tavernelli, I.; Coutinho-Neto, M. D.; Rothlisberger, U. *J. Chem. Theory Comput.* **2007**, *3*, 1673.

(42) Antony, J.; Grimme, S. *Phys. Chem. Chem. Phys.* **2006**, *8*, 5287.

(43) Goerigk, L.; Grimme, S. *J. Chem. Theory Comput.* **2010**, *6*, 107.

(44) Goerigk, L.; Grimme, S. *J. Chem. Theory Comput.* **2011**, *7*, 291.

(45) Dreuw, A.; Weisman, M.; Head-Gordon, M. *J. Phys. Chem.* **2003**, *119*, 2943.

(46) Serrano-Andrés, L.; Fülscher, M. *J. Am. Chem. Soc.* **1998**, *120*, 10912.

(47) Tawada, Y.; Tsuneda, T.; Yanagisawa, S.; Yanai, T.; Hirao, K. *J. Chem. Phys.* **2004**, *120*, 8425.

(48) Vydrov, O. A.; Scuseria, G. E. *J. Chem. Phys.* **2006**, *125*, 234109.

(49) Yanai, T.; Tew, D. P.; Handy, N. C. *Chem. Phys. Lett.* **2004**, *393*, 51.

(50) Peach, M. J. G.; Benfield, P.; Helgaker, T.; Tozer, D. J. *J. Chem. Phys.* **2008**, *128*, 044118.

(51) Chai, J.-D.; Head-Gordon, M. *J. Chem. Phys.* **2008**, *128*, 084106.

(52) Chai, J.-D.; Head-Gordon, M. *Phys. Chem. Chem. Phys.* **2008**, *10*, 6615.

(53) Jacquemin, D.; Perpète, E. A.; Ciofini, I.; Adamo, C. *Theor. Chem. Acc.* **2011**, *128*, 127.

(54) Grimme, S.; Neese, F. *J. Chem. Phys.* **2007**, *127*, 154116.

(55) Goerigk, L.; Moellmann, J.; Grimme, S. *Phys. Chem. Chem. Phys.* **2009**, *11*, 4611.

(56) Schwabe, T.; Grimme, S. *Phys. Chem. Chem. Phys.* **2007**, *9*, 3397.

(57) Frisch, M. J.; Trucks, G. W.; Schlegel, H. B.; Scuseria, G. E.; Robb, M. A.; Cheeseman, J. R.; Scalmani, G.; Barone, V.; Mennucci, B.; Petersson, G. A.; Nakatsuji, H.; Caricato, M.; Li, X.; Hratchian, H. P.; Izmaylov, A. F.; Bloino, J.; Zheng, G.; Sonnenberg, J. L.; Hada, M.; Ehara, M.; Toyota, K.; Fukuda, R.; Hasegawa, J.; Ishida, M.; Nakajima, T.; Honda, Y.; Kitao, O.; Nakai, H.; Vreven, T.; Montgomery, J. A., Jr.; Peralta, J. E.; Ogliaro, F.; Bearpark, M.; Heyd, J. J.; Brothers, E.; Kudin, K. N.; Staroverov, V. N.; Kobayashi, R.; Normand, J.; Raghavachari, K.; Rendell, A.; Burant, J. C.; Iyengar, S. S.; Tomasi, J.; Cossi, M.; Rega, N.; Millam, J. M.; Klene, M.; Knox, J. E.; Cross, J. B.; Bakken, V.; Adamo, C.; Jaramillo, J.; Gomperts, R.; Stratmann, R. E.; Yazyev, O.; Austin, A. J.;

Cammi, R.; Pomelli, C.; Ochterski, J. W.; Martin, R. L.; Morokuma, K.; Zakrzewski, V. G.; Voth, G. A.; Salvador, P.; Dannenberg, J. J.; Dapprich, S.; Daniels, A. D.; Farkas, O.; Foresman, J. B.; Ortiz, J. V.; Cioslowski, J.; Fox, D. J. *Gaussian 09*, revision A.02; Gaussian, Inc.: Wallingford, CT, 2009.

(58) Neese, F. *ORCA 2.7.0*; University of Bonn, Bonn, Germany; http://www.thch.uni-bonn.de/tc/orca/.

(59) Dunning, T. H., Jr. *J. Chem. Phys.* **1989**, *90*, 1007.

(60) Becke, A. D. *J. Chem. Phys.* **1993**, *98*, 5648.

(61) Lee, C.; Yang, W.; Parr, R. G. *Phys. Rev. B* **1988**, *37*, 785.

(62) Grimme, S. *J. Chem. Phys.* **2006**, *124*, 034108.

(63) Zhao, Y.; Truhlar, D. G. *J. Phys. Chem. A* **2006**, *110*, 13126.

(64) Boys, S. F.; Bernardi, F. *Mol. Phys.* **1970**, *19*, 553.

(65) Weigend, F.; Häser, M. *Theor. Chem. Acc.* **1997**, *97*, 331.

(66) Weigend, F.; Häser, M.; Patzelt, H.; Ahlrichs, R. *Chem. Phys. Lett.* **1998**, *294*, 143.

(67) Andersson, K.; Malmqvist, P.-Å.; Roos, B. *J. Chem. Phys.* **1992**, *96*, 1218.

(68) Andersson, K.; Roos, B. Part I, Advanced Series in Physical Chemistry. *Modern Electron Structure Theory*; Yarkony, R., Ed.; World Scientific, Singapore, 1995; Vol. 2, p 55.

(69) Roos, B.; Fülscher, M. P.; Malmqvist, P.-Å.; Merchán, M.; Serrano-Andrés, L. *Quantum Mechanical Electronic Structure Calculations with Chemical Accuracy*; S. R. Langhoff, Ed.; Kluwer Academic, Dordrecht, The Netherlands, 1995, p 357.

(70) Malmqvist, P.-Å. *Int. J. Quantum Chem.* **1986**, *30*, 479.

(71) Malmqvist, P.-Å.; Roos, B. *Chem. Phys. Lett.* **1989**, *155*, 189.

(72) Aquilante, F.; De Vico, L.; Ferré, N.; Ghigo, G.; Malmqvist, P.-Å.; Pedersen, T.; Pitonak, M.; Reiher, M.; Roos, B. O.; Serrano-Andrés, L.; Urban, M.; Veryazov, V.; Lindh, R. *J. Comput. Chem.* **2010**, *31*, 224.

(73) Head-Gordon, M.; Rico, R. J.; Oumi, M.; Lee, T. J. *Chem. Phys. Lett.* **1994**, *219*, 21.

(74) Sini, G.; Sears, J. S.; Brédas, J.-L. *J. Chem. Theory Comput.* **2011**, *7*, 602.

(75) Riley, K. E.; Pitonak, M.; Cerny, J.; Hobza, P. *J. Chem. Theory Comput.* **2010**, *6*, 66.

(76) Riley, K. E.; Pitonak, M.; Jurecka, P.; Hobza, P. *Chem. Rev.* **2011**, *110*, 5023.

(77) Mulliken, R. S. *J. Am. Chem. Soc.* **1950**, *72*, 600.

(78) Breneman, C. M.; Wiberg, K. B. *J. Comput. Chem.* **1990**, *11*, 361.

(79) Karthikeyan, S.; Sedlak, R.; Hobza, P. *J. Phys. Chem. A*, DOI: 10.1021/jp1112476.

(80) The charges are calculated at the MP2 level because the spin component scaled procedure is only applied to correct the energy.

(81) Tsuzuki, S.; Uchimaru, T.; Mikami, M. *J. Phys. Chem. A* **2006**, *110*, 2027.

(82) Brédas, J. L. *J. Chem. Phys.* **1985**, *82*, 3808.

(83) Aragó, J.; Viruela, P. M.; Ortí, E. *J. Mol. Struct. (Theochem)* **2009**, *912*, 27.

(84) Aragó, J.; Viruela, P. M.; Ortí, E.; Osuna, R. M.; Vercelli, B.; Zotti, G.; Hernández, V.; López Navarrete, J. T.; Henssler, J. T.; Matzger, A. J.; Suzuki, Y.; Yamaguchi, S. *Chem.—Eur. J.* **2010**, *16*, 5481.

(85) Aragó, J.; Viruela, P. M.; Gierschner, J.; Ortí, E.; Milián-Medina, B. *Phys. Chem. Chem. Phys.* **2011**, *13*, 1457.

(86) Sancho-García, J. C.; Pérez-Jiménez, A. J. *Phys. Chem. Chem. Phys.* **2007**, *9*, 5874.

(87) Stein, T.; Kronik, L.; Baer, R. *J. Am. Chem. Soc.* **2009**, *131*, 2818.

(88) Li, R.; Zheng, J.; Truhlar, D. G. *Phys. Chem. Chem. Phys.* **2010**, *12*, 12697.